Received: 31 May 2024 | Revised: 5 September 2024 | Accepted: 6 September 2024

DOI: 10.1002/pamm.202400187

RESEARCH ARTICLE

A rational ansatz for the approximation of Koopman eigenfunctions

Ulrich J. Römer | **Margarete Breitenhuber**

Institute of Engineering Mechanics, Karlsruhe Institute of Technology, Karlsruhe, Germany

Correspondence
Ulrich J. Römer, Institute of Engineering Mechanics, Karlsruhe Institute of Technology, Karlsruhe, Germany.
Email: ulrich.roemer@kit.edu

Abstract

Koopman operator theory offers a basis for the systematic transformation and linearization of complex dynamical systems. We propose a method to approximate eigenfunctions of the Koopman operator for sufficiently smooth, deterministic and autonomous dynamical systems with hyperbolic fixed points in an equation-based context. Approximations of the eigenfunctions are obtained in form of a rational ansatz whose coefficients are determined by minimizing a residual through a bi-quadratic optimization problem. In addition, we consider an extension of the Hartman-Grobman theorem, which was first proposed by Lan and Mezić in 2013, as a linear constraint. The implementation for a damped pendulum shows that the approach works in general, however, the optimization problem is non-convex and thus sensible w. r. t. initial conditions, and increases proportional to the number of ansatz functions to the power of four.

1 | INTRODUCTION

The Koopman operator as a tool to analyze and linearize dynamical systems has seen a lot of attention and research interest in the last two decades [1]. While many in the Koopman operator community have used it as a basis for data driven modeling approaches built on methods such as *Dynamic Mode Decomposition* (DMD) [2], *Extended Dynamic Mode Decomposition* (EDMD) [3] and further variants and improvements thereof [4], the Koopman operator also offers additional insights into the dynamics of systems for which there already is a mathematical model in the form of a nonlinear ordinary differential equation.

Given state variables $\mathbf{x} \in \mathcal{M} \subset \mathbb{R}^n$, the vector field $\mathbf{f} : \mathcal{M} \to T\mathcal{M}$, $\mathbf{f} \in C^2(\mathcal{M})$ defines an autonomous dynamical system by the ordinary differential equation

$$\frac{\mathrm{d}\mathbf{x}}{\mathrm{d}t} =: \dot{\mathbf{x}} = \mathbf{f}(\mathbf{x}) \,. \tag{1}$$

For any initial condition $\mathbf{x}(0) = \mathbf{x}_0$, the Picard-Lindelöf theorem [5] gives existence and uniqueness of a solution on some time interval $t \in (-a, a)$, $a > 0$, which we call the flow $\mathbf{x}(t) = \mathbf{S}(\mathbf{x}_0, t) =: \mathbf{S}^t(\mathbf{x}_0)$. The one parametric set of flow maps $\mathbf{S}^t : \mathcal{M} \to \mathcal{M}$, $\mathbf{S}^t : \mathbf{x}(0) \mapsto \mathbf{x}(t)$ defines a continuous parametric curve in phase space $\mathcal{M}$ for any initial condition $\mathbf{x}(0) = \mathbf{x}_0$.

An *observable* $g \in \mathcal{V}$ is any function $g : \mathcal{M} \to \mathbb{C}$ that maps the state $\mathbf{x}$ to a scalar. Well-known examples for observables in the context of dynamic systems are: any state x_i, an energy, a momentum, a Lyapunov function, a modal coordinate,

etc. We presume that $\mathcal{V}$ is a linear function space and define the *Koopman operator group*—often simply referred to as *the Koopman operator*—as the composition with the flow map

$$\mathcal{K}^t g := g \circ \mathbf{S}^t \,. \tag{2}$$

While the flow map $\mathbf{S}^t : \mathbf{x}(0) \mapsto \mathbf{x}(t)$ maps states onto states, elements $\mathcal{K}^t : \mathcal{V} \to \mathcal{V}$, $g \mapsto \tilde{g}^t$ of the Koopman operator group map functions onto functions. Since it is just the composition with the flow map, this operation may also be expressed as $\tilde{g}^t(\mathbf{x}_0) = g(\mathbf{S}^t(\mathbf{x}_0))$, $\forall \mathbf{x}_0 \in \mathcal{M}$. Since $\mathcal{K}^t$ is a one parametric group of operators with the easily verifiable property

$$\mathcal{K}^{t_2}\mathcal{K}^{t_1} g = \mathcal{K}^{t_1+t_2} g = \mathcal{K}^{t_2+t_1} g = \mathcal{K}^{t_1}\mathcal{K}^{t_2} g \,, \tag{3}$$

the *infinitesimal generator*—sometimes called *Lie operator* or *Kolmogorov backward operator*—

$$\mathcal{G} = \lim_{t \to 0^+} \frac{\mathcal{K}^t - \mathcal{I}}{t} \rightsquigarrow \mathcal{K}^t = \exp(\mathcal{G}t), \tag{4}$$

where $\mathcal{I}$ is the identity operator, can be used to generate any group element through the exponential mapping. Since $\mathcal{V}$ is presumed to be a linear function space, the Koopman operator

$$\mathcal{K}^t(g_1 + \alpha g_2) = \mathcal{K}^t g_1 + \alpha \mathcal{K}^t g_2 \quad (g_1, g_2 \in \mathcal{V}, \alpha \in \mathbb{C}) \tag{5}$$

is linear and thus amenable to spectral analysis. However, since $\dim(\mathcal{V}) = \infty$, the price that we pay for the desirable property of linearity is the infinite dimensionality of the function space $\mathcal{V}$. Even if $\mathcal{K}^t$ only has a point spectrum—that is, no continuous and no residual spectrum—there is an infinite number of eigenfunctions ϕ_i and corresponding eigenvalues λ_i that satisfy

$$\mathcal{K}^t \phi_i = \mathrm{e}^{\lambda_i t}\phi_i \quad \Leftrightarrow \quad \mathcal{G}\phi_i = \lambda_i \phi_i \,. \tag{6}$$

Definition (2) implies

$$\mathcal{K}^t(\phi_i\phi_j) = (\phi_i \circ \mathbf{S}^t)(\phi_j \circ \mathbf{S}^t) = (\mathcal{K}^t\phi_i)(\mathcal{K}^t\phi_j) = \mathrm{e}^{\lambda_i t}\phi_i \mathrm{e}^{\lambda_j t}\phi_j = \mathrm{e}^{(\lambda_i+\lambda_j)t}\phi_i\phi_j \tag{7}$$

that is, the product $\phi_k = \phi_i\phi_j$ of any two eigenfunctions ϕ_i and ϕ_j is again an eigenfunction with eigenvalue $\lambda_k = \lambda_i + \lambda_j$. Since Equation (4) implies $\mathcal{G}\phi_i = \mathrm{d}\phi_i/\mathrm{d}t = \dot{\phi}_i$, Equation (6) gives

$$\dot{\phi}_i = \lambda_i \phi_i \,. \tag{8}$$

Therefore, the constant function $\phi_0(\mathbf{x}) = 1 = \text{const.}$ is always an eigenfunction with eigenvalue $\lambda_0 = 0$. Presuming that the reciprocal $\phi_j = 1/\phi_i \in \mathcal{V}$ is contained in $\mathcal{V}$, Equation (7) implies that ϕ_j is also an eigenfunction of $\mathcal{K}^t$ and $\mathcal{G}$, and the corresponding eigenvalue is $\lambda_j = -\lambda_i$.

In the case where the dynamic system given by Equation (1) has fixed points, the infinite spectrum of the Koopman operator group has a lattice structure that is generated by relation (7) from $n_\mathrm{p} \geq n$ so-called *principal eigenfunctions* [6]. These principal eigenfunctions may be derived by an extension of the Hartman-Grobman theorem as first proposed by Lan and Mezić in 2013 [7]. We summarize and paraphrase this in the following way: given an isolated fixed point $\mathbf{x}^*$ of the dynamic system with $\mathbf{f}(\mathbf{x}^*) = \mathbf{0}$, the linearization around $\mathbf{x}^*$ with $\mathbf{y} = \mathbf{x} - \mathbf{x}^*$, $\mathbf{y} \in \mathbb{R}^n$ is

$$\dot{\mathbf{y}} = \mathbf{A}\,\mathbf{y} \quad \text{with} \quad \mathbf{A} = \nabla_{\mathbf{x}}\mathbf{f}|_{\mathbf{x}=\mathbf{x}^*} \,. \tag{9}$$

Here, we presume $\mathbf{A} \in \mathbb{R}^{n\times n}$ to be semi-simple (the general case is treated in [6]) and to have left-eigenvectors $\boldsymbol{\ell}_i$ and corresponding eigenvalues λ_i that we collect in the matrices

$$\mathbf{L} = [\boldsymbol{\ell}_1 \ \dots \ \boldsymbol{\ell}_n] \,, \quad \boldsymbol{\Lambda} = \mathrm{diag}\{\lambda_1, \dots, \lambda_n\} \,. \tag{10}$$

The n principal eigenfunctions of the linearized system (9) are then

$$\varphi_i = \boldsymbol{\ell}_i^{\mathsf{H}} \mathbf{y} \quad \text{with} \quad \dot{\varphi}_i = \lambda_i \varphi_i \tag{11}$$

via Equation (8), where $\boldsymbol{\ell}_i^{\mathsf{H}}$ is the complex conjugate transpose of $\boldsymbol{\ell}_i$. Presuming a *hyperbolic fixed point* where all eigenvalues have a non-zero real part $\Re\lambda_i \neq 0$, $\forall i \in \{1, \dots, n\}$, the Hartman-Grobman theorem establishes the existence of a C^1-diffeomorphism $\mathbf{y} = \mathbf{h}(\mathbf{x})$ from an open neighborhood $\mathcal{N}$ of the fixed point $\mathbf{x}^* \in \mathcal{N}$ onto an open set $\mathcal{W}$ that contains the origin, such that

$$\mathbf{h} \circ \mathbf{S}^t(\mathbf{x}) = \mathrm{e}^{\mathbf{A}t} \mathbf{h}(\mathbf{x}) \,, \tag{12}$$

that is, $\mathbf{h} : \mathcal{M} \supset \mathcal{N} \to \mathcal{W} \subset \mathbb{R}^n$ maps trajectories of (1) near the fixed point onto trajectories of (9) near the origin and preserves the parametrization by time [7]. Setting $\mathbf{k} = \mathbf{L}^{\mathsf{H}} \mathbf{h}$ yields

$$\mathbf{k} \circ \mathbf{S}^t(\mathbf{x}) = \mathrm{e}^{\mathbf{\Lambda}t} \mathbf{k}(\mathbf{x}) = \mathrm{diag}\{\mathrm{e}^{\lambda_1 t}, \dots, \mathrm{e}^{\lambda_n t}\} \mathbf{k}(\mathbf{x}) \,, \tag{13}$$

meaning $\mathbf{k}$ contains n eigenfunctions of the Koopman operator of the original nonlinear system (1). As described in ref. [6], these eigenfunctions $\phi_i(\mathbf{x}) = k_i(\mathbf{x})$ that so-far exist only in the open neighborhood $\mathcal{N}$ of the fixed point $\mathbf{x}^* \in \mathcal{N}$ can be extended to the whole basin of attraction $\mathcal{B}$ of $\mathbf{x}^*$. Furthermore, since $\nabla_{\mathbf{x}} \mathbf{h}|_{\mathbf{x}=\mathbf{x}^*} = \mathbf{I}$,

$$\nabla_{\mathbf{x}} \mathbf{k}|_{\mathbf{x}=\mathbf{x}^*} \mathbf{y} = \mathbf{L}^{\mathsf{H}} \mathbf{y} = \boldsymbol{\varphi}(\mathbf{y}) \,, \tag{14}$$

that is, the linearization of the eigenfunctions around the fixed point $\mathbf{x}^*$ is equal to the eigenfunctions of the linearized system (9) with the same eigenvalues $\lambda_1, \dots, \lambda_n$. These principal eigenfunctions $\phi_i(\mathbf{x}) = k_i(\mathbf{x})$ and their corresponding eigenvalues λ_i with $i \in \{1, \dots, n\}$ generate the lattice type point spectrum via Equation (7) [6].

In the remainder of this manuscript, we present an approach for the approximation of principal Koopman eigenfunctions in the basin of attraction of a hyperbolic fixed point of a dynamic system. We use a rational ansatz where both the numerator and denominator are linear combinations of ansatz functions to simultaneously approximate not only the principal eigenfunctions, but also their reciprocals by minimizing a suitable residual. We use a damped pendulum—a two-dimensional system with a stable focus and an unstable saddle point—for a first implementation of this approach to assess its feasibility and to identify requirements for future research.

2 | APPROACH

To approximate principal eigenfunctions $\phi_i(\mathbf{x})$ of the Koopman operator $\mathcal{K}^t$ and its infinitesimal generator $\mathcal{G}$ via Equation (6), we make the rational ansatz

$$\tilde{\phi}_i(\mathbf{x}) = \frac{p(\mathbf{x})}{q(\mathbf{x})} = \frac{\boldsymbol{\xi}_p^{\mathsf{T}} \boldsymbol{\Psi}(\mathbf{x})}{\boldsymbol{\xi}_q^{\mathsf{T}} \boldsymbol{\Psi}(\mathbf{x})} \,. \tag{15}$$

Here, $\boldsymbol{\Psi}(\mathbf{x}) = [\psi_1(\mathbf{x}) \;\; \dots \;\; \psi_m(\mathbf{x})]^{\mathsf{T}}$ is a set of m real-valued ansatz functions $\psi_i : \mathbb{R}^n \to \mathbb{R}$ which are the same for the numerator and the denominator, and $\boldsymbol{\xi}_p = [\xi_{p1} \dots \xi_{pm}]^{\mathsf{T}}$ and $\boldsymbol{\xi}_q = [\xi_{q1} \dots \xi_{qm}]^{\mathsf{T}}$ are m complex-valued coefficients $\boldsymbol{\xi}_p \in \mathbb{C}^m$ and $\boldsymbol{\xi}_q \in \mathbb{C}^m$ for the numerator $p : \mathbb{R}^n \to \mathbb{C}$ and the denominator $q : \mathbb{R}^n \to \mathbb{C}$, respectively. Since $\tilde{\phi}_i$ is an approximation for the eigenfunction ϕ_i, it does not satisfy Equation (8) exactly, but leads to the error

$$e(\mathbf{x}) = \lambda_i \, \tilde{\phi}_i(\mathbf{x}) - \nabla_{\mathbf{x}} \tilde{\phi}_i(\mathbf{x}) \, \mathbf{f}(\mathbf{x}) \,, \tag{16}$$

where

$$\dot{\tilde{\phi}}_i(\mathbf{x}) = \nabla_{\mathbf{x}} \tilde{\phi}_i(\mathbf{x}) \, \dot{\mathbf{x}} = \nabla_{\mathbf{x}} \tilde{\phi}_i(\mathbf{x}) \, \mathbf{f}(\mathbf{x}) \tag{17}$$

follows from the chain rule. We use the linearization of the nonlinear system (1) at an hyperbolic fixed point $\mathbf{x}^*$ to determine the eigenvalues λ_i. By the introduced extension of the Hartman-Grobman theorem, the ansatz for the corresponding principal eigenfunction must also satisfy the linearization condition

$$\nabla_{\mathbf{x}}\tilde{\phi}_i(\mathbf{x})\big|_{\mathbf{x}=\mathbf{x}^*}(\mathbf{x}-\mathbf{x}^*) = \boldsymbol{\ell}_i^{\mathsf{H}}(\mathbf{x}-\mathbf{x}^*)\,. \tag{18}$$

The gradient of the ansatz is

$$\nabla_{\mathbf{x}}\tilde{\phi}_i(\mathbf{x}) = \frac{1}{q^2(\mathbf{x})}(q(\mathbf{x})\,\nabla_{\mathbf{x}}p(\mathbf{x}) - p(\mathbf{x})\,\nabla_{\mathbf{x}}q(\mathbf{x}))\,, \tag{19}$$

which motivates the residual

$$\begin{aligned}\rho(\mathbf{x}) &= q^2(\mathbf{x})\,e(\mathbf{x})\\ &= \lambda_i\,p(\mathbf{x})\,q(\mathbf{x}) - (q(\mathbf{x})\,\nabla_{\mathbf{x}}p(\mathbf{x}) - p(\mathbf{x})\,\nabla_{\mathbf{x}}q(\mathbf{x}))\,\mathbf{f}(\mathbf{x})\\ &= \boldsymbol{\xi}_q^{\mathsf{T}}(\lambda_i\,\boldsymbol{\Psi}(\mathbf{x})\,\boldsymbol{\Psi}^{\mathsf{T}}(\mathbf{x}) - \boldsymbol{\Psi}(\mathbf{x})\,(\nabla_{\mathbf{x}}\boldsymbol{\Psi}(\mathbf{x})\,\mathbf{f}(\mathbf{x}))^{\mathsf{T}} + (\nabla_{\mathbf{x}}\boldsymbol{\Psi}(\mathbf{x})\,\mathbf{f}(\mathbf{x}))\,\boldsymbol{\Psi}^{\mathsf{T}}(\mathbf{x}))\boldsymbol{\xi}_p\,,\end{aligned} \tag{20}$$

which is bilinear in the coefficients $\boldsymbol{\xi}_p$ and $\boldsymbol{\xi}_q$. For the latter implementation, we note that since the ansatz functions $\boldsymbol{\Psi} : \mathbb{R}^n \to \mathbb{R}^m$ are real-valued, the real and imaginary parts of $\rho(\mathbf{x}) = \rho_{\mathrm{Re}}(\mathbf{x}) + \mathrm{i}\rho_{\mathrm{Im}}(\mathbf{x})$ can be determined by splitting the eigenvalue $\lambda_i = \lambda_{\mathrm{Re}} + \mathrm{i}\lambda_{\mathrm{Im}}$ and the coefficients $\boldsymbol{\xi}_p = \boldsymbol{\xi}_{p\mathrm{Re}} + \mathrm{i}\boldsymbol{\xi}_{p\mathrm{Im}}$ and $\boldsymbol{\xi}_q = \boldsymbol{\xi}_{q\mathrm{Re}} + \mathrm{i}\boldsymbol{\xi}_{q\mathrm{Im}}$ into their respective real and imaginary parts. We use the Kronecker product [8] to define

$$\boldsymbol{\eta}(\boldsymbol{\xi}_p, \boldsymbol{\xi}_q) = \begin{bmatrix}\boldsymbol{\xi}_{p\mathrm{Re}}\\ \boldsymbol{\xi}_{p\mathrm{Im}}\end{bmatrix} \otimes \begin{bmatrix}\boldsymbol{\xi}_{q\mathrm{Re}}\\ \boldsymbol{\xi}_{q\mathrm{Im}}\end{bmatrix}, \quad \boldsymbol{\eta} \in \mathbb{R}^{(2m)^2} \tag{21}$$

and to express the residual as

$$\rho(\mathbf{x}) = \rho_{\mathrm{Re}}(\mathbf{x}) + \mathrm{i}\rho_{\mathrm{Im}}(\mathbf{x}) = \boldsymbol{\zeta}_{\mathrm{Re}}^{\mathsf{T}}(\mathbf{x})\,\boldsymbol{\eta}(\boldsymbol{\xi}_p, \boldsymbol{\xi}_q) + \mathrm{i}\boldsymbol{\zeta}_{\mathrm{Im}}^{\mathsf{T}}(\mathbf{x})\,\boldsymbol{\eta}(\boldsymbol{\xi}_p, \boldsymbol{\xi}_q)\,, \tag{22}$$

where the column matrices $\boldsymbol{\zeta}_{\mathrm{Re}}(\mathbf{x})$ and $\boldsymbol{\zeta}_{\mathrm{Im}}(\mathbf{x})$ follow from the real and imaginary part of the matrix in the bracket in Equation (20) by rearranging its entries according to the calculation rules of the Kronecker product [8]. The unknown coefficients for the ansatz (15) are determined by minimizing the integral of the squared magnitude of the residual $\rho(\mathbf{x})$ over some finite domain $\Omega \subset \mathcal{M}$

$$\begin{aligned}&\int_\Omega |\rho(\mathbf{x})|^2 \mathrm{d}\mathbf{x} = \int_\Omega (\rho_{\mathrm{Re}}(\mathbf{x}))^2 \mathrm{d}\mathbf{x} + \int_\Omega (\rho_{\mathrm{Im}}(\mathbf{x}))^2 \mathrm{d}\mathbf{x} = (\boldsymbol{\eta}(\boldsymbol{\xi}_p, \boldsymbol{\xi}_q))^{\mathsf{T}}\,\mathbf{B}\,\boldsymbol{\eta}(\boldsymbol{\xi}_p, \boldsymbol{\xi}_q)\\ &\text{with}\quad \mathbf{B} = \int_\Omega (\boldsymbol{\zeta}_{\mathrm{Re}}(\mathbf{x})\,\boldsymbol{\zeta}_{\mathrm{Re}}^{\mathsf{T}}(\mathbf{x}) + \boldsymbol{\zeta}_{\mathrm{Im}}(\mathbf{x})\,\boldsymbol{\zeta}_{\mathrm{Im}}^{\mathsf{T}}(\mathbf{x}))\mathrm{d}\mathbf{x}, \quad \mathbf{B} \in \mathbb{R}^{(2m)^2\times(2m)^2}\end{aligned} \tag{23}$$

while enforcing the linearization condition (18). To do this, we also multiply the linearization condition by $q^2(\mathbf{x}^*)$ to derive the constraints

$$\begin{aligned} & & q^2(\mathbf{x}^*)\,\nabla_{\mathbf{x}}\tilde{\phi}_i\big|_{\mathbf{x}=\mathbf{x}^*} &= q^2(\mathbf{x}^*)\,\boldsymbol{\ell}_i^{\mathsf{H}}\\ &\Leftrightarrow\quad & q(\mathbf{x}^*)\,\nabla_{\mathbf{x}}p(\mathbf{x})|_{\mathbf{x}=\mathbf{x}^*} - p(\mathbf{x}^*)\,\nabla_{\mathbf{x}}q(\mathbf{x})|_{\mathbf{x}=\mathbf{x}^*} - q^2(\mathbf{x}^*)\,\boldsymbol{\ell}_i^{\mathsf{H}} &= \mathbf{0}\\ \Leftrightarrow\quad & \boldsymbol{\xi}_q^{\mathsf{T}}\left(\boldsymbol{\Psi}(\mathbf{x}^*)\,\boldsymbol{\xi}_p^{\mathsf{T}}\,\nabla_{\mathbf{x}}\boldsymbol{\Psi}(\mathbf{x})|_{\mathbf{x}=\mathbf{x}^*} - \nabla_{\mathbf{x}}\boldsymbol{\Psi}(\mathbf{x})|_{\mathbf{x}=\mathbf{x}^*}\,\boldsymbol{\xi}_p^{\mathsf{T}}\,\boldsymbol{\Psi}(\mathbf{x}^*) - \boldsymbol{\Psi}(\mathbf{x}^*)\,\boldsymbol{\Psi}^{\mathsf{T}}(\mathbf{x}^*)\,\boldsymbol{\xi}_q\,\boldsymbol{\ell}_i^{\mathsf{H}}\right) &= \mathbf{0}\\ &\Rightarrow\quad \left(\boldsymbol{\Psi}(\mathbf{x}^*)\,\boldsymbol{\xi}_p^{\mathsf{T}} - \boldsymbol{\Psi}^{\mathsf{T}}(\mathbf{x}^*)\,\boldsymbol{\xi}_p\right)\,\nabla_{\mathbf{x}}\boldsymbol{\Psi}(\mathbf{x})|_{\mathbf{x}=\mathbf{x}^*} - \boldsymbol{\xi}_q^{\mathsf{T}}\,\boldsymbol{\Psi}(\mathbf{x}^*)\,\boldsymbol{\Psi}(\mathbf{x}^*)\,\boldsymbol{\ell}_i^{\mathsf{H}} &= \mathbf{0}\,,\end{aligned} \tag{24}$$

which are linear in the coefficients $\boldsymbol{\xi}_p$ and $\boldsymbol{\xi}_q$.

In summary, our approach results in the constrained optimization problem

$$\begin{aligned} &\min_{\boldsymbol{\xi}_p,\boldsymbol{\xi}_q} \frac{1}{2}\boldsymbol{\eta}^\mathsf{T}(\boldsymbol{\xi}_p,\boldsymbol{\xi}_q)\,\mathbf{B}\,\boldsymbol{\eta}(\boldsymbol{\xi}_p,\boldsymbol{\xi}_q) \\ &\text{subject to} \quad (\boldsymbol{\Psi}(\mathbf{x}^*)\,\boldsymbol{\xi}_p^\mathsf{T} - \boldsymbol{\Psi}^\mathsf{T}(\mathbf{x}^*)\,\boldsymbol{\xi}_p)\,\nabla_\mathbf{x}\boldsymbol{\Psi}(\mathbf{x})|_{\mathbf{x}=\mathbf{x}^*} - \boldsymbol{\xi}_q^\mathsf{T}\,\boldsymbol{\Psi}(\mathbf{x}^*)\,\boldsymbol{\Psi}(\mathbf{x}^*)\,\boldsymbol{\ell}_i^\mathsf{H} = \mathbf{0}\,, \\ &\qquad\quad \boldsymbol{\xi}_q^\mathsf{T}\,\boldsymbol{\Psi}(\mathbf{x}^*) = 1\,, \end{aligned} \tag{25}$$

where the last constraint—setting the denominator to one at the fixed point $\mathbf{x}^*$—is introduced to enforce finite coefficients. Otherwise, any numerical optimization scheme reduces the magnitude of all coefficients to arbitrarily small values in such a way that Equation (24) is satisfied, and the objective is below the specified numerical tolerance.

Equation (25) is a nonlinear optimization problem with linear constraints which we solve iteratively via *IPOPT* [9]. Note that for this purpose, the real-valued matrices $\mathbf{B}$, $\boldsymbol{\Psi}(\mathbf{x}^*)$ and $\nabla_\mathbf{x}\boldsymbol{\Psi}(\mathbf{x})|_{\mathbf{x}=\mathbf{x}^*}$ can be precomputed, that is, the costly integrals in Equation (23) need only be calculated once.

Furthermore, note that applying the procedure above to the reciprocal ansatz function $\tilde{\phi}_j = 1/\tilde{\phi}_i$, that is, for switched numerator and denominator, and eigenvalue $\lambda_j = -\lambda_i$ gives the residual $-\rho(\mathbf{x})$. That means that the solution to the optimization problem (25) is not just the best approximation for the eigenfunction $\phi_i \approx \tilde{\phi}_i$, but simultaneously for its reciprocal $1/\phi_i$.

For a proof-of-concept, we apply this approach to a damped pendulum with states $\mathbf{x} \in \mathbb{S} \times \mathbb{R}$ and dynamics

$$\begin{bmatrix} \dot{x}_1 \\ \dot{x}_2 \end{bmatrix} = \begin{bmatrix} x_2 \\ -2Dx_2 - \sin x_1 \end{bmatrix}, \tag{26}$$

where we set $D = 0.1$ for all the numerical results below. This system has a stable fixed point $\mathbf{x}_1^* = \mathbf{0}$ at the origin, and an unstable saddle point at $\mathbf{x}_2^* = [\pi\ 0]^\mathsf{T}$. The linearization around the stable fixed point at the origin with $\mathbf{y} = \mathbf{x} - \mathbf{x}_1^*$ gives the linearized system

$$\begin{bmatrix} \dot{y}_1 \\ \dot{y}_2 \end{bmatrix} = \begin{bmatrix} 0 & 1 \\ -1 & -2D \end{bmatrix} \begin{bmatrix} y_1 \\ y_2 \end{bmatrix} \tag{27}$$

with eigenvalues, left-eigenvectors and principal eigenfunctions

$$\lambda_{1,2} = -D \pm \mathrm{i}\sqrt{1 - D^2}\,, \tag{28a}$$

$$\boldsymbol{\ell}_{1,2}^\mathsf{H} = [1 \quad -\lambda_{1,2}]\,, \tag{28b}$$

$$\varphi_{1,2} = y_1 - \lambda_{1,2} y_2\,. \tag{28c}$$

Since the phase space $\mathcal{M} = \mathbb{S} \times \mathbb{R}$ of the pendulum is a cylinder, we choose harmonic ansatz functions in x_1 and polynomials in x_2, and the rectangular integration domain $\Omega = (-\pi, \pi] \times [-2, 2]$. We compare results for an increasing order (one *I*, two *II* or three *III*) of the ansatz functions with

$$\boldsymbol{\Psi}_I(\mathbf{x}) = [1 \quad \cos x_1 \quad \sin x_1]^\mathsf{T} \otimes [1 \quad x_2]^\mathsf{T} = [1 \quad \cos x_1 \quad \sin x_1 \quad x_2 \quad x_2 \cos x_1 \quad x_2 \sin x_1]^\mathsf{T}\,, \tag{29a}$$

$$\boldsymbol{\Psi}_{II}(\mathbf{x}) = [1 \quad \cos x_1 \quad \sin x_1 \quad \cos(2x_1) \quad \sin(2x_1)]^\mathsf{T} \otimes [1 \quad x_2 \quad x_2^2]^\mathsf{T}\,, \tag{29b}$$

$$\boldsymbol{\Psi}_{III}(\mathbf{x}) = [1 \quad \cos x_1 \quad \sin x_1 \quad \cos(2x_1) \quad \sin(2x_1) \quad \cos(3x_1) \quad \sin(3x_1)]^\mathsf{T} \otimes [1 \quad x_2 \quad x_2^2 \quad x_2^3]^\mathsf{T}\,. \tag{29c}$$

For this proof-of-concept implementation, the integrals in Equation (23) are solved symbolically in *Mathematica* [10]. Note that

$$\dim(\mathbf{B}) = 16m^4\,, \tag{30}$$

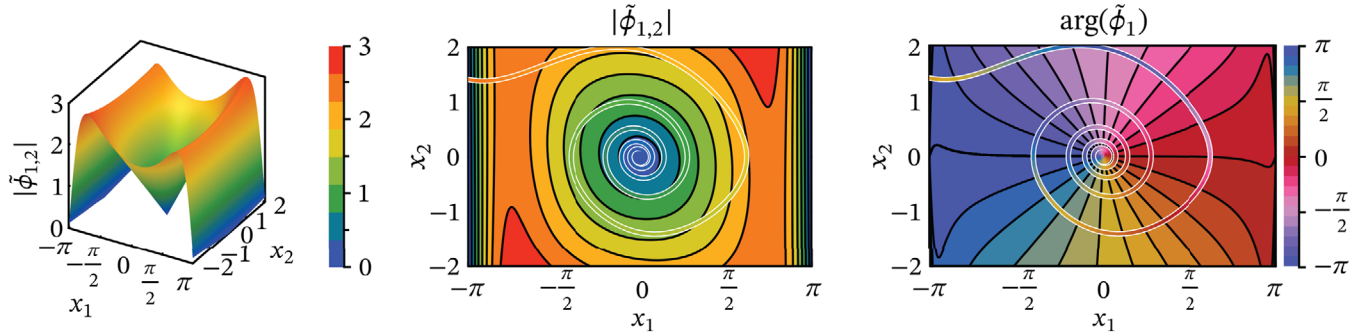

FIGURE 1 Koopman eigenfunction approximation $\tilde{\phi}_1(\mathbf{x}) \approx \phi_1(\mathbf{x})$ with $m_I = 6$ ansatz functions $\mathbf{\Psi}_I(\mathbf{x})$ via Equation (29a) as solution of the optimization problem (25) with initial conditions via Equation (31). Exact values along one trajectory overlayed.

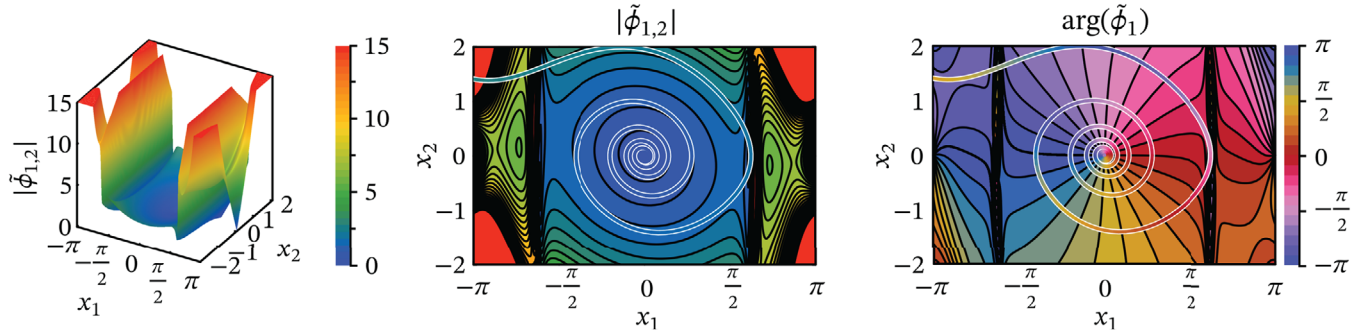

FIGURE 2 Koopman eigenfunction approximation $\tilde{\phi}_1(\mathbf{x}) \approx \phi_1(\mathbf{x})$ with $m_{II} = 15$ ansatz functions $\mathbf{\Psi}_{II}(\mathbf{x})$ via Equation (29b) as solution of the optimization problem (25) with initial conditions via Equation (31). Exact values along one trajectory overlayed.

that is, a slight increase of m leads to a substantial increase in computation time and memory requirements, which is why only ansatz functions up to order three are considered. We note that for all three implemented ansatz orders, about two thirds (65.1 % – 67.7 %) of the entries in $\mathbf{B}$ are zero.

3 | RESULTS

An approximate solution for the optimization problem (25) is determined with *Mathematica*'s implementation of *IPOPT* (function *FindMinimum* with option *Method* →*"IPOPT"*). Since we use a gradient-based solver for a (non-convex) bi-quadratic optimization problem with linear constraints, the result depends on the initial conditions of the optimization variables $\boldsymbol{\xi}_p$ and $\boldsymbol{\xi}_q$. Since no further information is available, all three orders are initialized with

$$\boldsymbol{\xi}_{p,\text{init0}} = \mathbf{0} \quad \text{and} \quad \boldsymbol{\xi}_{q,\text{init0}} = \mathbf{0}\,. \tag{31}$$

The results for these approximations are displayed in Figures 1, 2 and 3. Both magnitude and phase of all three approximations match the expected behavior in the vicinity of the origin. This behavior is enforced by our method by means of the linearization constraint in Equation (24). However, all three approximations deteriorate with increasing distance from the origin. While we expect both the magnitude and phase of $\phi_1(\mathbf{x})$ to increase or decrease monotonically along solution trajectories, there are local maxima of the magnitude in the vicinity of $x_1 \approx \pm 2$ in clear violation of this. Furthermore, since trajectories with initial conditions close to the unstable fixed point $\mathbf{x}_2^*$ require a long time to come close to the stable fixed point $\mathbf{x}_1^*$, we expect a singularity of the magnitude at $\lim_{\mathbf{x}\to\mathbf{x}_2^*} |\phi_1(\mathbf{x})| \to \infty$. Instead, the magnitude of all three approximations decreases to zero.

To enforce the expected qualitative properties of the eigenfunctions approximations at the unstable fixed point, we augment the optimization problem (25) by adding another constraint, namely that the denominator

$$q(\mathbf{x}_2^*) = \boldsymbol{\xi}_q^\top \mathbf{\Psi}(\mathbf{x}_2^*) = 0\,. \tag{32}$$

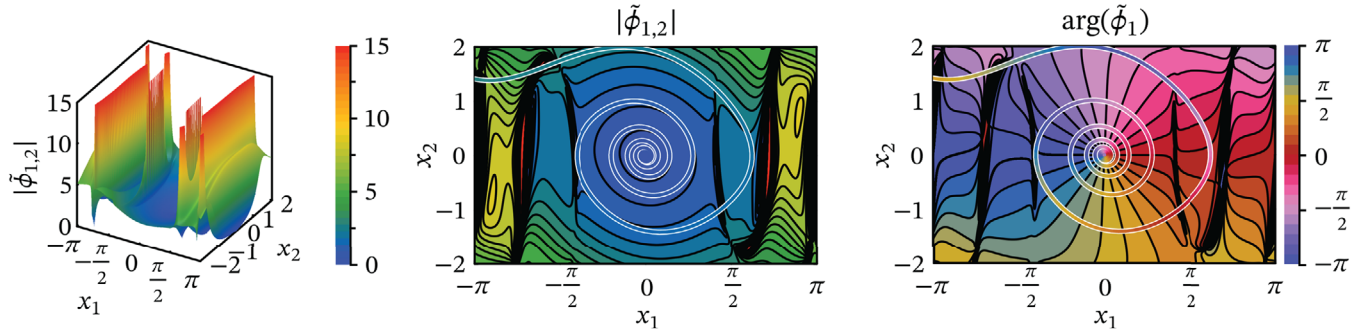

FIGURE 3 Koopman eigenfunction approximation $\tilde{\phi}_1(\mathbf{x}) \approx \phi_1(\mathbf{x})$ with $m_{III} = 28$ ansatz functions $\mathbf{\Psi}_{III}(\mathbf{x})$ via Equation (29c) as solution of the optimization problem (25) with initial conditions via Equation (31). Exact values along one trajectory overlayed.

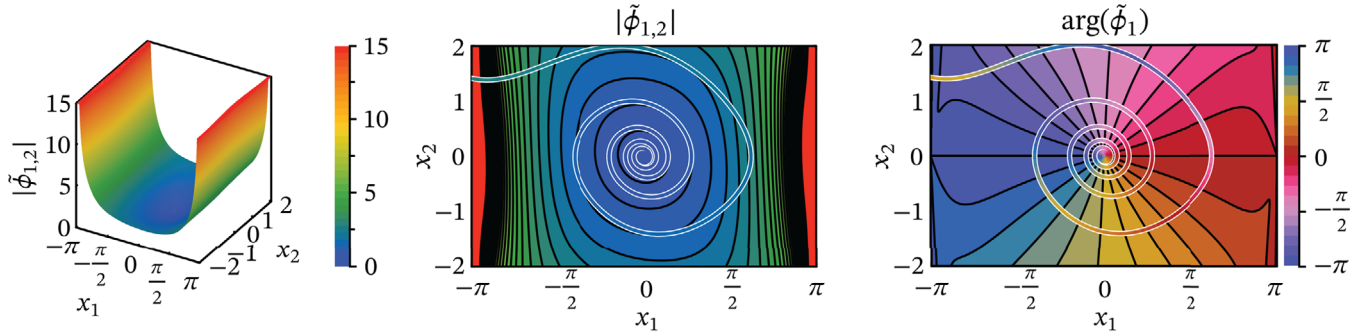

FIGURE 4 Koopman eigenfunction approximation $\tilde{\phi}_1(\mathbf{x}) \approx \phi_1(\mathbf{x})$ with $m_I = 6$ ansatz functions $\mathbf{\Psi}_I(\mathbf{x})$ via Equation (29a) as solution of the optimization problem (33) with initial conditions via Equation (31). Exact values along one trajectory overlayed.

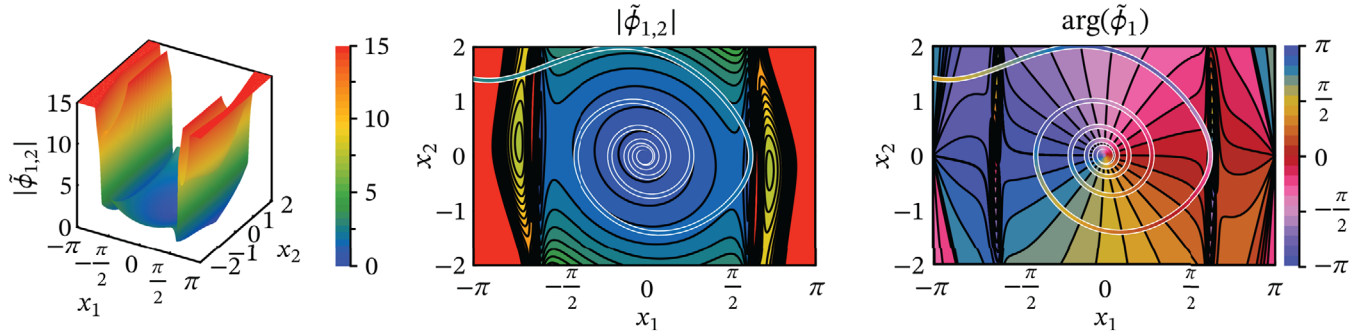

FIGURE 5 Koopman eigenfunction approximation $\tilde{\phi}_1(\mathbf{x}) \approx \phi_1(\mathbf{x})$ with $m_{II} = 15$ ansatz functions $\mathbf{\Psi}_{II}(\mathbf{x})$ via Equation (29b) as solution of the optimization problem (33) with initial conditions via Equation (31). Exact values along one trajectory overlayed.

The augmented optimization problem is then

$$\begin{aligned} &\min_{\boldsymbol{\xi}_p, \boldsymbol{\xi}_q} \frac{1}{2} \boldsymbol{\eta}^\mathsf{T}(\boldsymbol{\xi}_p, \boldsymbol{\xi}_q)\, \mathbf{B}\, \boldsymbol{\eta}(\boldsymbol{\xi}_p, \boldsymbol{\xi}_q) \\ \text{subject to} \quad &(\mathbf{\Psi}(\mathbf{x}_1^*)\, \boldsymbol{\xi}_p^\mathsf{T} - \mathbf{\Psi}^\mathsf{T}(\mathbf{x}_1^*)\, \boldsymbol{\xi}_p)\, \nabla_{\mathbf{x}} \mathbf{\Psi}(\mathbf{x})|_{\mathbf{x}=\mathbf{x}_1^*} - \boldsymbol{\xi}_q^\mathsf{T}\, \mathbf{\Psi}(\mathbf{x}_1^*)\, \mathbf{\Psi}(\mathbf{x}_1^*)\, \boldsymbol{\mathcal{V}}_i^\mathsf{H} = \mathbf{0}\,, \\ &\boldsymbol{\xi}_q^\mathsf{T}\, \mathbf{\Psi}(\mathbf{x}_1^*) = 1\,, \\ &\boldsymbol{\xi}_q^\mathsf{T}\, \mathbf{\Psi}(\mathbf{x}_2^*) = 0\,, \end{aligned} \tag{33}$$

and the results for the initialization via Equation (31) are depicted in Figures 4, 5 and 6. While the order one approximation in Figure 4 matches the qualitative behavior of both magnitude and phase, the higher order approximations still

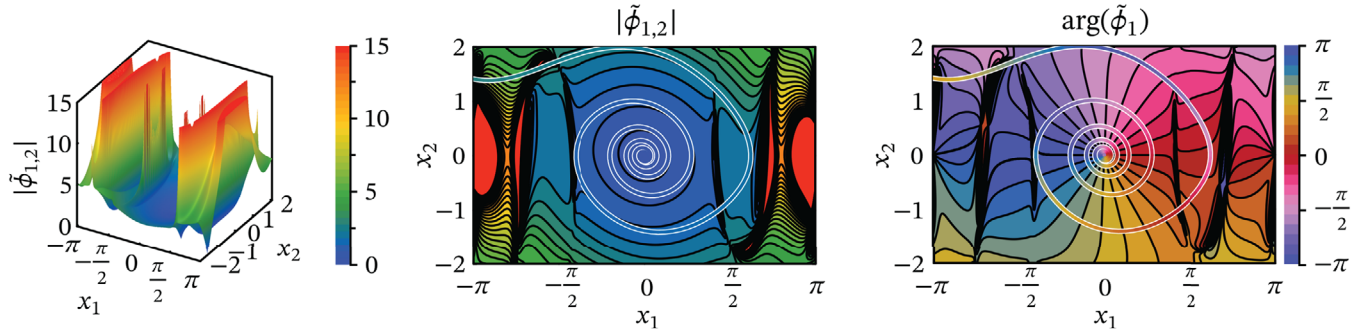

FIGURE 6 Koopman eigenfunction approximation $\tilde{\phi}_1(\mathbf{x}) \approx \phi_1(\mathbf{x})$ with $m_{III} = 28$ ansatz functions $\mathbf{\Psi}_{III}(\mathbf{x})$ via Equation (29c) as solution of the optimization problem (33) with initial conditions via Equation (31). Exact values along one trajectory overlayed.

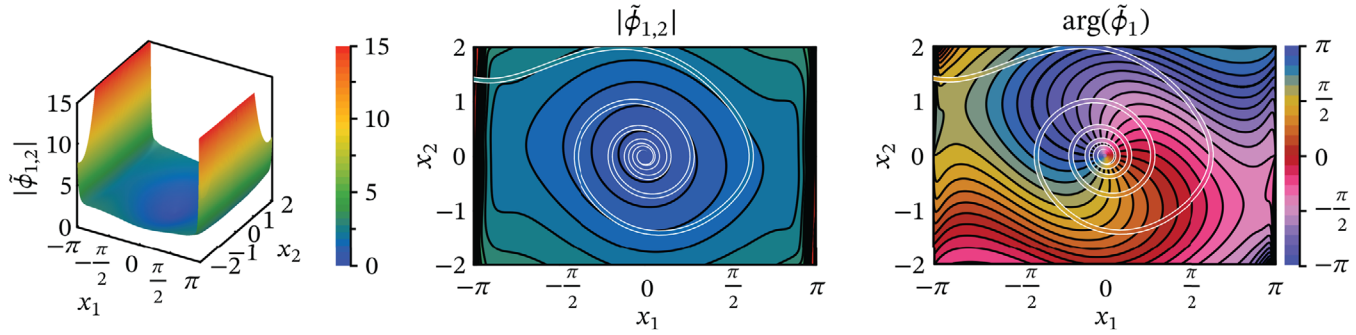

FIGURE 7 Koopman eigenfunction approximation $\tilde{\phi}_1(\mathbf{x}) \approx \phi_1(\mathbf{x})$ with $m_{III} = 28$ ansatz functions $\mathbf{\Psi}_{III}(\mathbf{x})$ via Equation (29c) as solution of the optimization problem (33) with initial conditions from the result in Figure 1. Exact values along one trajectory overlayed.

show unexpected behavior in the vicinity of $x_1 \approx \pm 2$. The reason for these poor solutions can be found in the initial conditions for the optimization, since the bi-quadratic optimization problem (33) with linear constraints is not convex and has several local minima. Trying all previous solutions as initial conditions for the order two and three ansatz functions, we find no improvement for the order two approximation in Figure 5. However, initializing the order three approximation with the solution from Figure 1 yields the result in Figure 7, which is better than all previous results, both qualitatively and quantitatively.

4 | CONCLUSION

A method to approximate Koopman eigenfunctions of sufficiently smooth, deterministic autonomous dynamics systems by the rational ansatz in Equation (15) is proposed. A proof-of-concept implementation with a damped pendulum shows that the coefficients in the rational ansatz can be determined by solving a bi-quadratic optimization problem with linear constraints. However, the size of this optimization problem increases proportional to the number of ansatz function by the power of four (cf. Equation (30)). In the investigated proof-of-concept implementation, about two thirds of the matrix entries for the bi-quadratic objective function are zero. We consider it very likely that with a higher dimension of the phase space $\mathcal{M}$, and corresponding combinations of ansatz functions generated by Kronecker products (cf. Equation (29)), the number of zero entries will further increase, and thus a high sparsity will be achieved with which the presented method could scale to higher-dimensional dynamic systems.

The results for the damped pendulum show a good approximation of the Koopman eigenfunction in the vicinity of the stable fixed point $\mathbf{x}_1^* = \mathbf{0}$. This is attributed to the linearization condition in Equation (18) which is enforced by the constraint via Equation (24) in the resulting constrained optimization problem. However, the approximation deteriorates further away from the origin and exhibits local maxima at all considered ansatz orders. Furthermore, the magnitude of the Koopman eigenfunction approximations goes to zero at the unstable fixed point, which is the opposite of what should happen. The proposed method offers the possibility to improve the approximation by adding further information in the

form of additional constraints in the optimization problem. In the present case, the expected singularity at the unstable fixed point is enforced by setting the value of the denominator there to zero.

Since the bi-quadratic optimization problem with linear constraints is non-convex, a further challenge is the proper initialization of any numerical optimization procedure in order to obtain qualitatively and quantitatively good approximations with the proposed approach. The only difference between the results in Figures 6 and 7 is the initialization of the respective optimization problem (33), which leads to much better results in the latter case. In future work, this could be addressed by using multi-modal optimization methods [11–14] to obtain suitable initializations for a gradient based method with fast local convergence.

ACKNOWLEDGMENTS

Open access funding enabled and organized by Projekt DEAL.

ORCID

Ulrich J. Römer https://orcid.org/0000-0002-6393-6063

REFERENCES

1. Brunton, S. L., Budišić, M., Kaiser, E., & Kutz, J. N. (2021). Modern Koopman theory for dynamical systems. *SIAM Review*, *64*(2), 229–340.
2. Schmid, P. J., & Sesterhenn, J. (2008). Dynamic mode decomposition of numerical and experimental data. *Bulletin of the American Physical Society*, *53*(15), 61st APS meeting, San Antonio, TX, p. 208.
3. Williams, M. O., Kevrekidis, I. G., & Rowley, C. W. (2015). A data–driven approximation of the koopman operator: Extending dynamic mode decomposition. *Journal of Nonlinear Science*, *25*, 1307–1346.
4. Schmid, P. J. (2022). Dynamic mode decomposition and its variants. *Annual Review of Fluid Mechanics*, *54*(1), 225–254.
5. Hairer, E., Wanner, G., & Nørsett, S. P. (1993). *Solving Ordinary Differential Equations I*. Springer Berlin Heidelberg.
6. Mezić, I. (2020). Spectrum of the Koopman operator, spectral expansions in functional spaces, and state-space geometry. *Journal of Nonlinear Science*, *30*, 2091–2145.
7. Lan, Y., & Mezić, I. (2013). Linearization in the large of nonlinear systems and Koopman operator spectrum. *Physica D: Nonlinear Phenomena*, *242*(1), 42–53.
8. Van Loan, C. F. (2000). The ubiquitous Kronecker product. *Journal of Computational and Applied Mathematics*, *123*(1–2), 85–100.
9. Wächter, A., & Biegler, L. T. (2006). On the implementation of a primal-dual interior point filter line search algorithm for large-scale nonlinear programming. *Mathematical Programming*, *106*(1), 25–57.
10. Mathematica (Version 14.0) [Computer software]. Wolfram Research Inc. https://www.wolfram.com/mathematica
11. Yang, X.-S. (2009). Firefly algorithms for multimodal optimization. In O. Watanabe, & T. Zeugmann (Eds.), *Lecture notes in computer science: Vol. 5792. Stochastic algorithms: Foundations and applications, proceedings of the 5th international symposium, SAGA 2009* (pp. 169–178). Springer-Verlag.
12. Barrera, J., & Coello, C. A. C. (2009). A review of particle swarm optimization methods used for multimodal optimization. In C. P. Lim, L. C. Jain, & S. Dehuri (Eds.), *Studies in computational intelligence: Vol. 248. Innovations in swarm intelligence*. Springer.
13. Qu, B. Y., Suganthan, P. N., & Liang, J. J. (2012). Differential evolution with neighborhood mutation for multimodal optimization. *IEEE Transactions on Evolutionary Computation*, *16*(5), 601–614.
14. Wang, Y., Li, H.-X., Yen, G. G., & Song, W. (2015). MOMMOP: Multiobjective optimization for locating multiple optimal solutions of multimodal optimization problems. *IEEE Transactions on Cybernetics*, *45*(4), 830–843.

How to cite this article: Römer, U. J., & Breitenhuber, M. (2024). A rational ansatz for the approximation of Koopman eigenfunctions. *Proceedings in Applied Mathematics and Mechanics*, e202400187. https://doi.org/10.1002/pamm.202400187